Electrical spin injection through dual ferromagnetic electrodes in nonlocal spin valves

Xi-guang Wang, Yao-zhuang Nie, Qing-lin Xia, and Guang-hua Guo*
School of Physics and Electronics, Central South University, Changsha, 410083, China

(Received 4 September 2018; revised manuscript received 24 October 2018; published 26 November 2018)

Spin injection efficiency has been a key factor for designing spintronic devices based on the lateral nonlocal spin valve. Here, we suggest a type of nonlocal spin valve in which the spin is injected electrically via dual ferromagnetic electrodes similar to a vertical spin valve and the spin detection is done by another ferromagnetic electrode. Using spin drift-diffusion theory, we study the spin injection, transport, and detection analytically and numerically. The results show that the spin injection efficiency can be enhanced significantly compared to the usual single ferromagnetic electrode injection, and thus the detected spin signal is increased greatly. Besides, by controlling the magnetization orientations of the two injecting ferromagnetic electrodes as well as the magnetization direction of the detection electrode, one can switch on and off the spin injection and thus form three or four output spin states. This feature is used for designing all spin-based three-state logic devices.

DOI: 10.1103/PhysRevB.98.184427

I. INTRODUCTION

Spin transport in magnetic nanostructures has been a key factor for designing spintronic devices [1–4]. Various types of spin transport phenomena have been reported, including spin pumping [5–7], spin Hall effect [8–13], spin Seebeck effect [14–16], and nonlocal spin injection (Refs. [11,17,18] and others). Also, in semiconductor heterostructures with spin-orbit interaction (such as the heterostructure grown from III-V semiconductor compounds), the spin-dependent tunneling was applied for pure electric injection and detection of spin-polarized currents [19–22]. Each phenomenon provides a unique insight into the spin manipulation, and related applications (for example, magnetic sensors, spin logic devices, and storage devices) have been proposed [2,4,23,24], among which the nonlocal lateral spin valves (NLSVs), with the abilities of separating charge and spin currents, have attracted a great amount of attention [11,17,18,25]. Comparing with "local" spin valves consisting of vertical stacks (two ferromagnetic metal layers, and nonmagnetic metal spacer in the middle), the NLSV is more propitious to design semiconductor spin devices, such as the spin field-effect transistor [26].

A typical NLSV structure consists of a nonmagnetic (NM) channel connected with two ferromagnetic (FM) electrodes. As shown in Fig. 1(a), spin is injected into the NM (N) from the first FM (F1), and the induced spin accumulation at the interface diffuses in the NM channel, forming a pure spin current. The second FM (F2) electrode is used to detect the spin current via an electric voltage. The spin injection efficiency and the voltage signal are two key indicators for NLSV. Usually, for the NLSV with FM/NM interface (i.e., transparent interface), the nonlocal resistance is only several milliohms, far smaller than the output of local vertical spin valves [27–31]. To increase the output voltage, the FM/insulator(I)/NM interface (i.e., tunnel junction) is suggested, and several hundred milliohms are achieved [32–35]. Further increasing the spin injection efficiency and effectively manipulating the spin transport are still goals for designing the NLSV and related devices [36,37].

In this work, we propose a type of NLSV structure as shown in Fig. 1(b). The spin is injected into NM channel via a vertical spin valve structure with two FM electrodes (F1 and F3) and detected by F2 electrode. We analytically study the spin injection, transport, and detection based on the spin drift-diffusion equations. We show that the spin injection efficiency and the nonlocal resistance are increased by two times compared with the usual NLSV structure with a single FM injecting electrode. Numerical simulations confirm the analytical results. Moreover, by manipulating the relative directions of the magnetizations of two injecting FM as well as the detecting FM electrodes, we can get three or four output states. This feature is exploited to design three-state logical gates.

II. THEORETICAL MODEL

The spin transport in FM electrodes and NM channel is studied based on the spin drift-diffusion equations which are given by the following equations [18]:

$$\nabla^2(\sigma_\uparrow\mu_\uparrow + \sigma_\downarrow\mu_\downarrow) = 0, \tag{1}$$

$$\nabla^2(\mu_\uparrow - \mu_\downarrow) = \frac{(\mu_\uparrow - \mu_\downarrow)}{\lambda^2}. \tag{2}$$

Here, μ_s is the electrochemical potential for spin channel $s = \uparrow$ or $\downarrow$, σ_s is the electrical conductivity, and λ is the spin diffusion length. The electrical conductivities in NM are spin independent, i.e., ${\sigma^N}_\uparrow = {\sigma^N}_\downarrow = 1/(2\rho_N)$, and ρ_N is resistivity. Those in ferromagnetic layers are spin dependent: ${\sigma^F}_{\uparrow(\downarrow)} = 1/\{2\rho_F[1-(+)\beta]\}$ for the FM with local magnetization along $\uparrow$, and ${\sigma^F}_{\uparrow(\downarrow)} = 1/\{2\rho_F[1+(-)\beta]\}$ when the

*guogh@mail.csu.edu.cn

 ©2018 American Physical Society

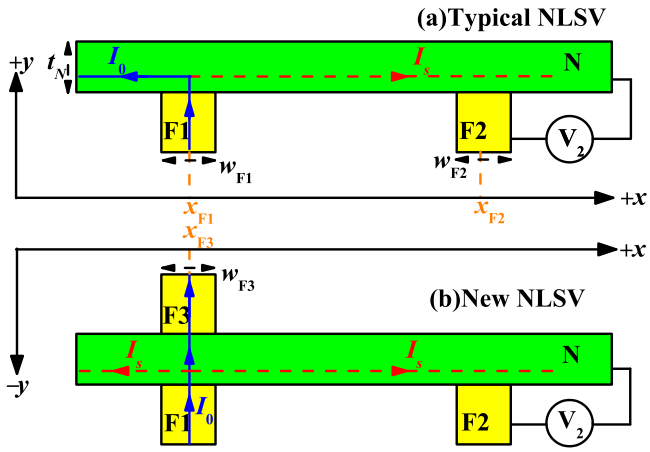

FIG. 1. (a) Sketch of the typical NLSV. Electric current I_0 flowing from F1 to the left side of NM channel generates a spin accumulation at F1/N interface. The spin current is detected by measuring the spin-dependent voltage V_2 between F2 and NM. (b) Sketch of the new NLSV with adding F3. Electric current I_0 flowing from F1 to the F3 generates a spin accumulation at the F1/N/F3 interface. The coordinates x_{F1}, x_{F2}, and x_{F3} represent the locations of F1, F2, and F3, respectively.

magnetization is along $\downarrow$. ρ_F is resistivity and β is the electric current polarization.

Inside each layer, the electrical current density j_s is determined by the gradient of the spin electrochemical potential,

$$j_{\uparrow(\downarrow)} = \frac{\sigma_{\uparrow(\downarrow)}}{e}\nabla\mu_{\uparrow(\downarrow)}. \tag{3}$$

Here, $e = |e|$ represents the electron charge. Across the FM/NM (or FM/I/NM) interface, the interfacial current density j_s^i is determined by

$$\mu_{\uparrow(\downarrow)}(y_+^i) - \mu_{\uparrow(\downarrow)}(y_-^i) = r_{\uparrow(\downarrow)}e[j_{\uparrow(\downarrow)}^i], \tag{4}$$

where y^i is the coordinate of the interface. For the interface with local magnetization $\mathbf{M}$ along $\uparrow$, the spin-dependent boundary resistance for a unit surface is $r_{\uparrow(\downarrow)} = 2r_b[1 - (+)\gamma]$, and for opposite magnetization $\mathbf{M}$ (along$\downarrow$), $r_{\uparrow(\downarrow)} = 2r_b[1 + (-)\gamma]$. Here, γ is the interfacial spin asymmetry coefficient, and r_b is the interface resistance parameter.

The spin current density j_{sp} and spin accumulation $d\mu$ are defined as $j_{sp} = j_\uparrow - j_\downarrow$ and $d\mu = (\mu_\uparrow - \mu_\downarrow)/2$, respectively. The $d\mu$ is detected electrically as a voltage drop in the detection terminal F2/N, and the nonlocal resistance is obtained as $R_s = \mu_{dif}/(|e| \times I_0)$. Here, $\mu_{dif} = [(\mu_\uparrow + \mu_\downarrow)/2]_{y=y(F2)} - [(\mu_\uparrow + \mu_\downarrow)/2]_{x=x(N)}$. $[(\mu_\uparrow + \mu_\downarrow)/2]_{x=x(N)}$ represents the total electrochemical potential at the right end of the NM layer, and $[(\mu_\uparrow + \mu_\downarrow)/2]_{y=y(F2)}$ is the potential at the end of the F2.

III. ANALYTICAL SOLUTION

In the following, the above spin drift-diffusion equations are solved analytically for the NLSV with double-FM injection electrodes as shown in Fig. 1(b). In the F1, F2, and F3 electrodes, the solutions of Eqs. (1) and (2) take the form

$$\begin{aligned}\mu_s^{F1} &= \bar{\mu}^{F1} - s(1 - s\beta)K_F^1 e^{y/\lambda_F},\\ \mu_s^{F2} &= \bar{\mu}^{F2} - s(1 - s\beta)K_F^2 e^{y/\lambda_F},\\ \mu_s^{F3} &= \bar{\mu}^{F3} - s(1 - s\beta)K_F^3 e^{-y/\lambda_F}.\end{aligned} \tag{5}$$

Here, the spin channel s equals $+(-)1$ for the electron spin parallel (antiparallel) to the local magnetizations $\boldsymbol{M}_{F1}$, $\boldsymbol{M}_{F2}$, and $\boldsymbol{M}_{F3}$. The K_F^i terms represent the spin accumulation in the Fi electrode near Fi/N interfaces ($i = 1$, 2, and 3). $\bar{\mu}^{F1} = (I_0/A_{F1})e\rho_F(1 - \beta^2)y + eV_1$ and $\bar{\mu}^{F3} = (I_0/A_{F3})e\rho_F(1 - \beta^2)y + eV_3$ are linear with y, representing the charge current I_0 in F1 and F3. The interface area $A_{F1} = w_{F1} \times w_N$ and $A_{F3} = w_{F2} \times w_N$. Here, w_{F1} and w_{F2} are the width of F1 and F2 along x, and w_N is the width of N along z. $\bar{\mu}^{F2} = eV_2$ is a constant potential with no charge current in F2. V_1, V_2, and V_3 are the voltage drops $(\bar{\mu}^F - \bar{\mu}^N)/e$ at the FM-NM interfaces. Combining Eq. (3), the spin current $I_{sc}^{Fi} = A_{Fi} \times j_{sp}$ is expressed as

$$\begin{aligned}I_{sc}^{F1} &= m_1\beta I_0 - \frac{m_1 A_{F1}}{\lambda_F e\rho_F}K_F^1 e^{y/\lambda_F},\\ I_{sc}^{F2} &= -\frac{m_2 A_{F2}}{\lambda_F e\rho_F}K_F^2 e^{y/\lambda_F},\\ I_{sc}^{F3} &= m_3\beta I_0 + \frac{m_3 A_{F3}}{\lambda_F e\rho_F}K_F^3 e^{-y/\lambda_F}.\end{aligned} \tag{6}$$

Here, $m_i = +(-)1$ for the Fi with local magnetization along $\uparrow(\downarrow)$. In the NM channel with thickness $t_N \ll \lambda_N$, the spin accumulation is almost uniform across the y axis, and thus μ_s only varies with x. The spin-dependent electrochemical potential has the form

$$\begin{aligned}\mu_s^N(x) = \bar{\mu}^N(x) - s\big(&K_N^1 e^{-|x-x_{F1}|/\lambda_N}\\ &+ K_N^2 e^{-|x-x_{F2}|/\lambda_N} + K_N^3 e^{-|x-x_{F3}|/\lambda_N}\big).\end{aligned} \tag{7}$$

Here $\bar{\mu}^N(x) = 0$ (ground level), and the second term on the right side describes the potential shift of spin-up ($s = 1$) and spin-down ($s = -1$) electrons. The K_N^i terms represent the spin accumulations near Fi/N interfaces. In general, the spin accumulation at the interface induces spin currents propagating in the $+x$ and $-x$ directions simultaneously in the NM channel. The continuity of the total spin current at junctions Fi/N gives $I_{sc}^{Fi/N}(x) = (2A_N/\lambda_N e\rho_N)K_N^i$. Here, the cross-sectional area $A_N = t_N \times w_N$.

Using the continuity conditions [18] for the spin and charge currents at the interfaces, we can determine analytically the variables K_F^i, K_N^i, V_1, V_2, and V_3 in Eqs. (5)–(7). Here, we focus on the output spin-dependent voltage V_2 at F2, and obtain the nonlocal resistance for the new NLSV,

$$R_s[\uparrow_{F1}\uparrow(\downarrow)_{F2}\downarrow_{F3}] = \frac{V_2}{I_0} = \frac{+(-)2R_N(e_1 + e_2)(p_{\gamma\beta} - c_\beta c_\gamma e_3)\big(c_\gamma\beta\frac{R_F}{R_N} + c_\beta\gamma\frac{R_I}{R_N}\big)^2}{p_{\gamma\beta}^3 - 4c_\gamma^3\frac{R_F^3}{R_N^3} - c_\beta^2 c_r^2\big(e_1^2 + e_2^2 + e_3^2\big)p_{\gamma\beta} + 2c_\beta^3 c_\gamma^3 e_1 e_2 e_3}, \tag{8a}$$

$$R_s[\uparrow_{\mathrm{F1}}\uparrow(\downarrow)_{\mathrm{F2}}\uparrow_{\mathrm{F3}}] = \frac{V_2}{I_0} = \frac{-(+)2R_N(e_1-e_2)(p_{\gamma\beta}+c_\beta c_\gamma e_3)\left(c_\gamma\beta\frac{R_F}{R_N}+c_\beta\gamma\frac{R_I}{R_N}\right)^2}{p_{\gamma\beta}^3-4c_\gamma^3\frac{R_F^3}{R_N^3}-c_\beta^2c_r^2\left(e_1^2+e_2^2+e_3^2\right)p_{\gamma\beta}+2c_\beta^3c_\gamma^3e_1e_2e_3}. \tag{8b}$$

Here, we introduce $p_{\gamma\beta} = 2c_\gamma R_F/R_N + 2c_\beta R_I/R_N + c_\gamma c_\beta$, $c_\beta = 1-\beta^2$, $c_\gamma = 1-\gamma^2$, $e_1 = e^{-|x_{\mathrm{F2}}-x_{\mathrm{F3}}|/\lambda_N}$, $e_2 = e^{-|x_{\mathrm{F2}}-x_{\mathrm{F1}}|/\lambda_N}$, and $e_3 = e^{-|x_{\mathrm{F3}}-x_{\mathrm{F1}}|/\lambda_N}$. $R_N = \rho_N\lambda_N/A_N$, $R_F = \rho_F(1-\beta^2)\lambda_F/A_F$, and $R_I = r_b(1-\gamma^2)/A_F$ are the NM, FM, and interface resistances, respectively. The same interface area $A_{\mathrm{F1}} = A_{\mathrm{F2}} = A_{\mathrm{F3}} = A_F$ is adopted to simplify the analytical results.

For tunnel junction interface ($R_I \gg R_F$), the results become

$$R_s[\uparrow_{\mathrm{F1}}\uparrow(\downarrow)_{\mathrm{F2}}\downarrow_{\mathrm{F3}}] = +(-)\frac{(e_1+e_2)}{2}\gamma^2R_N, \tag{9a}$$

$$R_s[\uparrow_{\mathrm{F1}}\uparrow(\downarrow)_{\mathrm{F2}}\uparrow_{\mathrm{F3}}] = -(+)\frac{(e_1-e_2)}{2}\gamma^2R_N. \tag{9b}$$

In the limit of transparent interface ($R_I \ll R_F$), the nonlocal resistances are obtained as

$$R_s[\uparrow_{\mathrm{F1}}\uparrow(\downarrow)_{\mathrm{F2}}\downarrow_{\mathrm{F3}}] = +(-)\frac{(e_1+e_2)\beta^2R_N\left(\frac{2R_F^2}{R_N^2}+\frac{c_\beta(1-e_3)R_F}{R_N}\right)}{c_\beta^2\left(3-e_1^2-e_2^2-e_3^2\right)+\frac{c_\beta^3R_N}{2R_F}\left(1+2e_1e_2e_3-e_1^2-e_2^2-e_3^2\right)}, \tag{10a}$$

$$R_s[\uparrow_{\mathrm{F1}}\uparrow(\downarrow)_{\mathrm{F2}}\uparrow_{\mathrm{F3}}] = -(+)\frac{(e_1-e_2)\beta^2R_N\left(\frac{2R_F^2}{R_N^2}+\frac{c_\beta(1+e_3)R_F}{R_N}\right)}{c_\beta^2\left(3-e_1^2-e_2^2-e_3^2\right)+\frac{c_\beta^3R_N}{2R_F}\left(1+2e_1e_2e_3-e_1^2-e_2^2-e_3^2\right)}. \tag{10b}$$

Apparently, R_s is independent of the interface R_i in the aforementioned limited cases.

For numerical calculations, material parameters corresponding to the Py/I/Cu system are adopted [18,31]. For the ferromagnetic Py layer, the spin diffusion length is $\lambda_F = 5\,\mathrm{nm}$, resistivity is $\rho_F = 100\,\mathrm{n\Omega\,m}$, and polarization is $\beta = 0.7$. For the Cu channel, the spin diffusion length is $\lambda_N = 700\,\mathrm{nm}$ and resistivity is $\rho_N = 2\,\mathrm{n\Omega\,m}$. The tunnel junction interface is described by a large enough interface resistance $r_b > 1\times10^{-12}\,\Omega\,\mathrm{m}^2$, and spin asymmetry coefficient $\gamma = 0.4$ is assumed.

The distributions of spin accumulation $d\mu$ are shown in Fig. 2. The geoparameters are $w_{\mathrm{F1}} = w_{\mathrm{F3}} = w_{\mathrm{F2}} = 40\,\mathrm{nm}$, $w_N = 100\,\mathrm{nm}$, and $t_N = 11\,\mathrm{nm}$. F1 and F3 are located at the same position, $x_{\mathrm{F1}} = x_{\mathrm{F3}} = 0$. The injected electric current density $j_0 = I_0/(w_{\mathrm{F1}}\times w_N)$ is set to be $1\times10^{12}\,\mathrm{A/m^2}$. One can control the spin accumulation by manipulating the relative directions of the magnetizations of the two injecting FM electrodes. When $\boldsymbol{M}_{\mathrm{F3}}$ is parallel to $\boldsymbol{M}_{\mathrm{F1}}$ [Fig. 2(b)], the injected spin from the F1 electrode easily transmits through the F1/I/N and N/I/F3 interfaces, and the accumulation is totally switched off. In the case that $\boldsymbol{M}_{\mathrm{F1}}$ and $\boldsymbol{M}_{\mathrm{F3}}$ are antiparallel with each other, most of the injected spin-polarized current is reflected by the N/I/F3 interface. As a result, a large spin accumulation $d\mu$ is generated in the N channel [Fig. 2(a)]. The obvious discontinuities at F1/I/N and N/I/F3 interfaces are caused by a very large interface resistance parameter r_b in Eq. (4). If $r_b = 0$, $d\mu$ is expected to be continuous at the interface. The injected spin accumulation diffuses in the NM channel and exhibits exponential decaying with distance as shown in Fig. 2(c). At F2/I/N, the tunnel junction interface makes $d\mu$ discontinuous, and the spin accumulation in N is not aborted by F2. ($d\mu \approx 0$ in F2 is not shown).

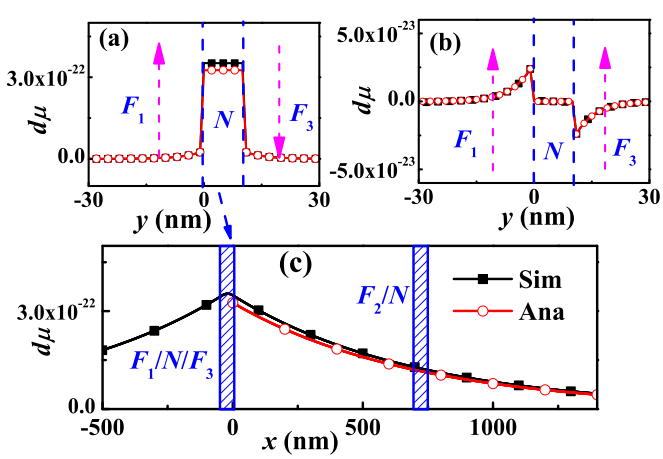

FIG. 2. Spatial variation of the spin accumulation $d\mu = (\mu\uparrow - \mu\downarrow)/2$ in the F1/I/N/I/F3 injection terminal for antiparallel (a) and parallel (b) $\boldsymbol{M}_{\mathrm{F1}}$ and $\boldsymbol{M}_{\mathrm{F3}}$, and in the NM channel (c). Solid squares and open circles are numerical and analytical results, respectively. Here, $x_{\mathrm{F1}} = x_{\mathrm{F3}} = 0$, and $x_{\mathrm{F2}} = 700\,\mathrm{nm}$.

The dependences of nonlocal resistances on the F2 position x_{F2} and the NM thickness t_N are shown in Figs. 3 and 4, respectively. Here, the results are calculated from Eq. (9), and $x_{\mathrm{F1}} = x_{\mathrm{F3}} = 0$. R_s varies inversely with t_N and decays exponentially with distance $L = x_{\mathrm{F2}} - x_{\mathrm{F1}}$ between the injecting and detecting electrodes. For $L = 700\,\mathrm{nm}$ ($x_{\mathrm{F2}} = 700\,\mathrm{nm}$ and $x_{\mathrm{F1}} = x_{\mathrm{F3}} = 0$) and $t_N = 11\,\mathrm{nm}$, $R_s[\uparrow_{\mathrm{F1}}\uparrow(\downarrow)_{\mathrm{F2}}\downarrow_{\mathrm{F3}}] = \pm77.5\,\mathrm{m\Omega}$ when the magnetizations $\boldsymbol{M}_{\mathrm{F1}}$ and $\boldsymbol{M}_{\mathrm{F3}}$ of two injection FM electrodes are antiparallel. When $\boldsymbol{M}_{\mathrm{F1}}$ and $\boldsymbol{M}_{\mathrm{F3}}$ are parallel, the spin injection is switched off, and $R_s(\uparrow_{\mathrm{F1}}\uparrow_{\mathrm{F2}}\uparrow_{\mathrm{F3}}) = R_s(\uparrow_{\mathrm{F1}}\downarrow_{\mathrm{F2}}\uparrow_{\mathrm{F3}}) = 0$ [$e_1 - e_2 = 0$ in

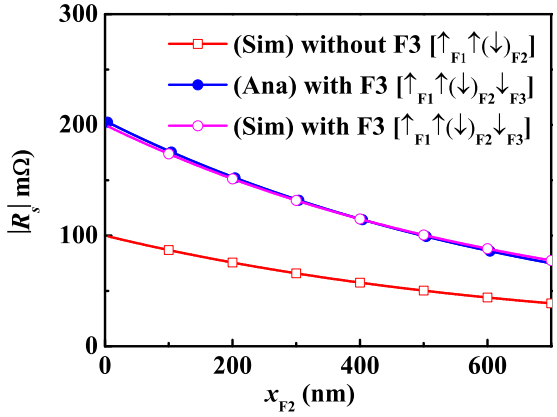

FIG. 3. Dependence of the nonlocal resistance amplitude $|R_s|$ on x_{F2} for the tunnel junction interface with (circles) and without (squares) F3. The solid and open dots are analytical and simulated results, respectively. Here, $x_{F1} = x_{F3} = 0$.

Eq. (9b)]. For comparison, the nonlocal resistances of the typical NLSV (i.e., without F3) are also calculated in Figs. 3 and 4. In this case the expression for nonlocal resistance is $R_s[\uparrow_{F1}\uparrow(\downarrow)_{F2}] = \pm\gamma^2 R_N e_2/2$ according to Ref. [18]. We see that the nonlocal resistances are enhanced by two times if the spin injection is implemented via two FM electrodes. The enhancement effect is reflected on the factor $(e_1 + e_2)$ in Eq. (9a).

By staggering positions of F1 and F3, i.e., $x_{F1} \neq x_{F3}$, we can further manipulate the spin accumulation and nonlocal resistance. Figure 5 shows the variation of nonlocal resistance R_s with the distance $\Delta x(=x_{F3} - x_{F1})$ between the two injecting FM electrodes F1 and F3. When the magnetizations of two injecting FM electrodes $\boldsymbol{M}_{F1}$ and $\boldsymbol{M}_{F3}$ are antiparallel, $R_s[\uparrow_{F1}\uparrow(\downarrow)_{F2}\downarrow_{F3}]$ increases (or decreases) with the F3 electrode approaching (or leaving) the detecting electrode F2 and reaches maximum at $x_{F3} = x_{F2}$. For parallel $\boldsymbol{M}_{F1}$ and $\boldsymbol{M}_{F3}$, the injected spin accumulation $d\mu$ from F1/N and F3/N interfaces cannot cancel each other when $x_{F1} \neq x_{F3}$, and negative $R_s(\uparrow_{F1}\uparrow_{F2}\uparrow_{F3})$ or positive $R_s(\uparrow_{F1}\downarrow_{F2}\uparrow_{F3})$ is detected by the

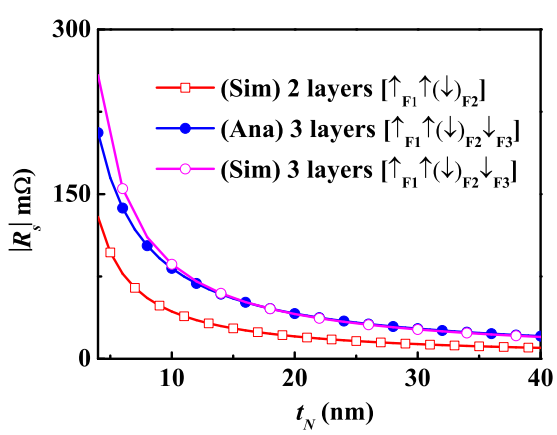

FIG. 4. Dependence of the nonlocal resistance amplitude $|R_s|$ on t_N for the tunnel junction interface with (circles) and without (squares) F3. The solid and open dots are analytical and simulated results, respectively. Here, $x_{F1} = x_{F3} = 0$, and $x_{F2} = 700$ nm.

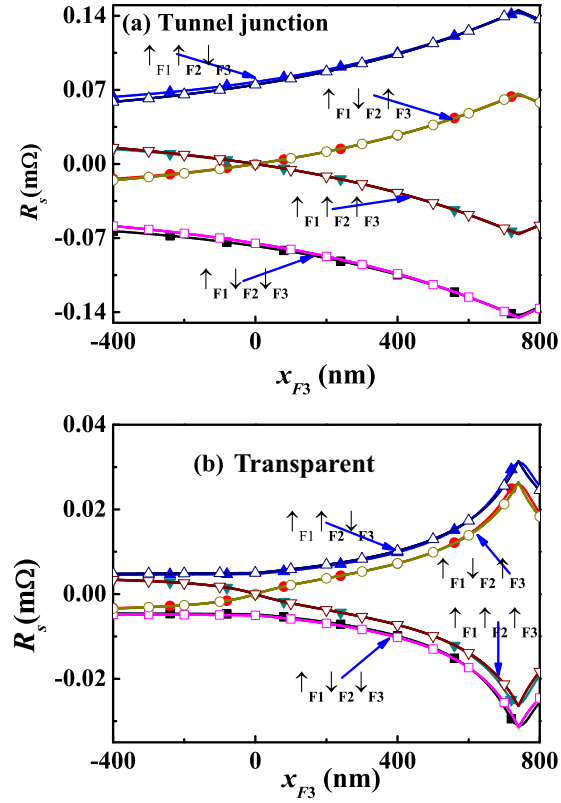

FIG. 5. Nonlocal resistance R_s as a function of the position x_{F3} of F3 for the tunnel junction interface (a) and transparent interface (b). Here, $x_{F1} = 0$ and $x_{F2} = 700$ nm. The solid and open dots are simulated and analytical results, respectively.

F2 electrode. Importantly, four different output states can be generated through controlling the magnetization directions of F1, F2, and F3 electrodes, which is very useful for designing spin logic devices.

It is noteworthy that for the transparent interface ($R_I \ll R_F$), Eq. 10(a) becomes $R_s[\uparrow_{F1}\uparrow(\downarrow)_{F2}\downarrow_{F3}] = +(-)(2\beta^2/c_\beta^2)R_N(R_F^2/R_N^2)e_2/(1-e_2^2)$ when $x_{F1} = x_{F3}$, which is the same as the expression $R_s[\uparrow_{F1}\uparrow(\downarrow)_{F2}]$ for the NLSV with single injecting FM electrode [18], meaning the spin injection is not significantly improved by adding F3 for the transparent interface. However, the spin injection via two FM electrodes still plays its role if the two electrodes are shifted from each other ($x_{F1} \neq x_{F3}$) as shown in Fig. 5(b). Here, $r_b = 0.25 \times 10^{-15}\,\Omega\,\mathrm{m}^2$ is used for transparent interface. Four output states are still attainable although R_s becomes much smaller. The influence of the interface resistance r_b on the nonlocal resistance is analytically calculated and shown in Fig. 6. For a small $r_b(<2 \times 10^{-13}\,\Omega\,\mathrm{m}^2)$, R_s increases rapidly with r_b. When r_b is in the region of tunnel junction ($r_b > 2 \times 10^{-13}\,\Omega\,\mathrm{m}^2$), R_s is mainly determined by R_N according to Eq. (9), and it barely changes in this region.

IV. SIMULATIONS

To confirm the analytical results, we perform simulations based on the spin drift-diffusion equations [Eqs. (1) and (2)] with the interface condition Eq. (4). The same material

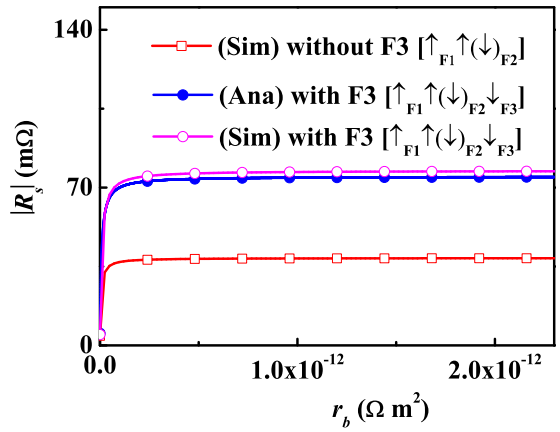

FIG. 6. Dependence of the nonlocal resistance amplitude $|R_s|$ on the interface resistance parameter r_b with (circles) and without (squares) F3. The solid and open dots are analytical and simulated results, respectively.

parameters in the analytical calculation are used here. The finite-difference method is adopted in simulations. The following assumptions are adopted: the thickness (y direction) of ferromagnetic electrodes (F1, F2, and F3) is much larger than the spin diffusion length λ_F, the width w_N (z direction) of NM channel is much smaller than λ_N, and the spin diffusions in the z direction are neglected. Under these assumptions, F1, F2, F3 electrodes and NM channel are discretized as two-dimensional ($x-y$ plane) wires with the cell size 1 nm × 1 nm. The electric current j_0 is injected from F1 into F3 electrodes, and $j_0 = j_\uparrow + j_\downarrow$. The boundary condition $j_{sp} = 0$ (i.e., $j_\uparrow = j_\downarrow$) is adopted for the vacuum interface. At the FM/NM interface, j_{sp} is determined by Eq. (4). All the simulation results are plotted in Figs. 2 –6 together with the analytical results. It can be seen that the simulations and analytical solutions are in full agreement, confirming the validity of the analytical results.

V. DESIGNING OF THREE-STATE LOGIC

We see that the spin injection via two FM electrodes not only raises the injecting efficiency significantly, but also provides three and even four output states. The latter is important for device design. For the typical NLSV with single injecting electrode F1 [Fig. 7(a)], the output signal (nonlocal resistance R_s) changes its sign when the magnetization $\boldsymbol{M}_{F1}$ of the input electrode and $\boldsymbol{M}_{F2}$ of the output electrode reorientate from parallel to antiparallel through external field B as shown in Fig. 7(a). Here, only two output states are attainable, i.e., $R_s[\uparrow_{F1}\uparrow_{F2}(\downarrow_{F2})] = +(-)|R_0|$. If the second injecting electrode is added to the NLSV, by manipulating the relative orientation of magnetizations of two injecting electrodes (F1 and F3) and detecting electrode (F2), we can obtain three output states as shown in Fig. 7(b), i.e., $R_s[\uparrow_{F1}\uparrow_{F2}(\downarrow_{F2})\downarrow_{F3}] = +(-)|R_0|$ and $R_s[\uparrow_{F1}\uparrow_{F2}\uparrow_{F3}] = R_s[\downarrow_{F1}\downarrow_{F2}\downarrow_{F3}] = 0$.

It has been well established that the dual output states of typical NLSV can be used for logical operation [23,24]. By defining two output states as state "0" and state "1," one can construct logic circuits based on this feature. Here, by adding the second injecting electrode F3, we are able to realize

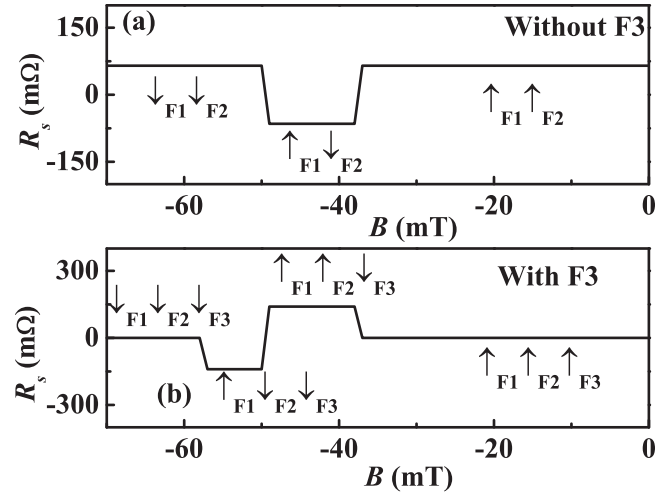

FIG. 7. Nonlocal resistance R_s as a function of magnetic field B for the NLSV without (a) and with (b) F3. Initially, the directions of $\boldsymbol{M}_{F1}$, $\boldsymbol{M}_{F2}$, and $\boldsymbol{M}_{F3}$ are all ↑. With increasing B, the magnetizations of F3, F2, and F1 are reversed one by one due to their different coercivities, giving three output states. Here, $x_{F1} = x_{F3} < x_{F2}$.

the other well-known logical unit, called "three-state logic" [38]. In some operations, one needs to remove the output (0 or 1 logical level) of logic unit from the circuit, without breaking the circuit. To achieve this purpose in the electric circuit, the electronic three-state logic needs to provide a high impendence state, in addition to the 0 and 1 states [38]. Here, the all spin-based three-state logic is easily achieved based on our design: In the case of antiparallel $\boldsymbol{M}_{F1}$ and $\boldsymbol{M}_{F3}$, the output can be negative (defined as 0 logical level) or positive (defined as 1 logical level), depending on the relative direction between $\boldsymbol{M}_{F1}$ and $\boldsymbol{M}_{F2}$. Switching to the parallel $\boldsymbol{M}_{F1}$ and $\boldsymbol{M}_{F3}$, the output voltage becomes zero independent of $\boldsymbol{M}_{F2}$, meaning the logical unit is removed from the circuit. This is equivalent to the high impendence state in the electric circuit. Besides, by shifting the two spin injecting electrodes apart from each other, one can achieve four output states as shown in Fig. 8.

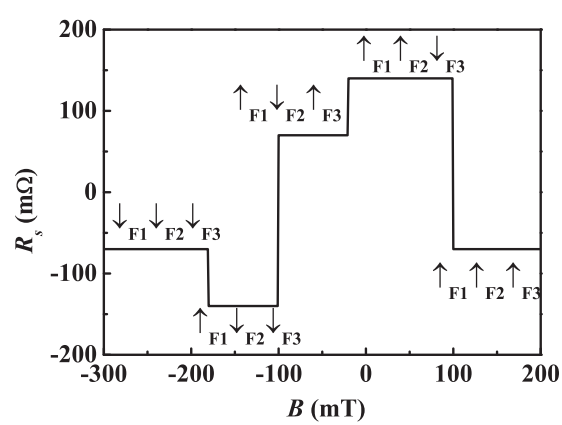

FIG. 8. Nonlocal resistance R_s as a function of magnetic field B. Here $x_{F2} = x_{F3} > x_{F1}$ and F2 and F3 are antiferromagnetic coupled. With decreasing magnetic field B, four output states appear sequentially. Each corresponds to different alignment of magnetizations $\boldsymbol{M}_{F1}$, $\boldsymbol{M}_{F2}$, and $\boldsymbol{M}_{F3}$.

The four spin states can be exploited to designing spintronic devices.

VI. CONCLUSION

To summarize, we proposed a NLSV structure with the vertical FM/I/NM/I/FM configuration in the spin injection terminal to improve the spin injection efficiency and the output spin signal. Adopting spin drift-diffusion simulation, we proved that the NLSV structure can enhance the output voltage by two times comparing with the usual NLSV with a single FM injecting electrode. Varying position of the added FM, the output can be further improved. Besides, our proposed NLSV can output three and even four different states, which is really desirable for designing spintronic devices, such as all spin-based three-state logic or four-state device.

ACKNOWLEDGMENTS

This work was supported by the National Natural Science Foundation of China (Grants No. 11704415, No. 11674400, and No. 11374373), and the Natural Science Foundation of Hunan Province of China (Grants No. 2018JJ3629 and No. 13JJ2004).

[1] M. I. Dyakonov, *Spin Physics in Semiconductors* (Springer-Verlag, Berlin, Heidelberg, 2017).
[2] C. Chappert, A. Fert, and F. N. Van Dau, Nat. Mater. **6**, 813 (2007).
[3] S. A. Wolf, D. D. Awschalom, R. A. Buhrman, J. M. Daughton, M. S. Von, M. L. Roukes, A. Y. Chtchelkanova, and D. M. Treger, Science **294**, 1488 (2001).
[4] I. Žutić, J. Fabian, and S. Das Sarma, Rev. Mod. Phys. **76**, 323 (2004).
[5] C. W. Sandweg, Y. Kajiwara, A. V. Chumak, A. A. Serga, V. I. Vasyuchka, M. B. Jungfleisch, E. Saitoh, and B. Hillebrands, Phys. Rev. Lett. **106**, 216601 (2011).
[6] Y. Tserkovnyak, A. Brataas, and G. E. W. Bauer, Phys. Rev. Lett. **88**, 117601 (2002).
[7] Y. Tserkovnyak, A. Brataas, G. E. W. Bauer, and B. I. Halperin, Rev. Mod. Phys. **77**, 1375 (2005).
[8] M. I. Dyakonov and V. I. Perel', Phys. Lett. A **35**, 459 (1971).
[9] M. I. Dyakonov and V. I. Perel', Sov. Phys. JETP Lett. **13**, 467 (1971).
[10] T. Jungwirth, J. Wunderlich, and K. Olejník, Nat. Mater. **11**, 382 (2012).
[11] T. Saburo and M. Sadamichi, Sci. Technol. Adv. Mater. **9**, 014105 (2008).
[12] Y. K. Kato, R. C. Myers, A. C. Gossard, and D. D. Awschalom, Science **306**, 1910 (2004).
[13] S. O. Valenzuela and M. Tinkham, Nature (London) **442**, 176 (2006).
[14] C. M. Jaworski, J. Yang, S. Mack, D. D. Awschalom, J. P. Heremans, and R. C. Myers, Nat. Mater. **9**, 898 (2010).
[15] K. Uchida, S. Takahashi, K. Harii, J. Ieda, W. Koshibae, K. Ando, S. Maekawa, and E. Saitoh, Nature (London) **455**, 778 (2008).
[16] J. Xiao, G. E. W. Bauer, K.-c. Uchida, E. Saitoh, and S. Maekawa, Phys. Rev. B **81**, 214418 (2010).
[17] M. Johnson and R. H. Silsbee, Phys. Rev. Lett. **55**, 1790 (1985).
[18] S. Takahashi and S. Maekawa, Phys. Rev. B **67**, 052409 (2003).
[19] V. I. Perel', S. A. Tarasenko, I. N. Yassievich, S. D. Ganichev, V. V. Bel'kov, and W. Prettl, Phys. Rev. B **67**, 201304 (2003).
[20] S. A. Tarasenko, V. I. Perel', and I. N. Yassievich, Phys. Rev. Lett. **93**, 056601 (2004).
[21] P. S. Alekseev, V. M. Chistyakov, and I. N. Yassievich, Semiconductors **40**, 1402 (2006).
[22] P. S. Alekseev, M. M. Glazov, and S. A. Tarasenko, Phys. Rev. B **89**, 155306 (2014).
[23] B. Behin-Aein, D. Datta, S. Salahuddin, and S. Datta, Nat. Nanotechnol. **5**, 266 (2010).
[24] H. Dery, P. Dalal, Ł. Cywiński, and L. J. Sham, Nature (London) **447**, 573 (2007).
[25] F. J. Jedema, A. T. Filip, and B. J. van Wees, Nature (London) **410**, 345 (2001).
[26] P. Chuang, S.-C. Ho, L. W. Smith, F. Sfigakis, M. Pepper, C.-H. Chen, J.-C. Fan, J. P. Griffiths, I. Farrer, H. E. Beere, G. A. C. Jones, D. A. Ritchie, and T.-M. Chen, Nat. Nanotechnol. **10**, 35 (2014).
[27] T. Kimura and Y. Otani, Phys. Rev. Lett. **99**, 196604 (2007).
[28] S. Satoshi, H. Susumu, T. Masayuki, K. Yuzo, and I. Hitoshi, Appl. Phys. Express **8**, 023103 (2015).
[29] Y. Ji, A. Hoffmann, J. E. Pearson, and S. D. Bader, Appl. Phys. Lett. **88**, 052509 (2006).
[30] S. Oki, S. Yamada, K. Tanikawa, K. Yamasaki, M. Miyao, and K. Hamaya, Appl. Phys. Lett. **103**, 212402 (2013).
[31] S. O. Valenzuela and M. Tinkham, Appl. Phys. Lett. **85**, 5914 (2004).
[32] G. Mihajlović, D. K. Schreiber, Y. Liu, J. E. Pearson, S. D. Bader, A. K. Petford-Long, and A. Hoffmann, Appl. Phys. Lett. **97**, 112502 (2010).
[33] Y. Fukuma, L. Wang, H. Idzuchi, S. Takahashi, S. Maekawa, and Y. Otani, Nat. Mater. **10**, 527 (2011).
[34] A. Vogel, J. Wulfhorst, and G. Meier, Appl. Phys. Lett. **94**, 122510 (2009).
[35] X. J. Wang, H. Zou, L. E. Ocola, and Y. Ji, Appl. Phys. Lett. **95**, 022519 (2009).
[36] A. Spiesser, H. Saito, Y. Fujita, S. Yamada, K. Hamaya, S. Yuasa, and R. Jansen, Phys. Rev. Appl. **8**, 064023 (2017).
[37] H. Idzuchi, S. Karube, Y. Fukuma, T. Aoki, and Y. Otani, Appl. Phys. Lett. **103**, 162403 (2013).
[38] P. Horowitz and W. Hill, *The Art of Electronics* (Cambridge University Press, Cambridge, England, 1989).